

~~CONFIDENTIAL~~

Copy 327
RM E52L02

NACA RM E52L02

TECH LIBRARY KAFB, NM
0143432



RESEARCH MEMORANDUM

FREE-FLIGHT PERFORMANCE OF A ROCKET-BOOSTED,
AIR-LAUNCHED 16-INCH-DIAMETER RAM-JET ENGINE
AT MACH NUMBERS UP TO 2.20

By John H. Disher, Robert C. Kohl, and Merle L. Jones

Lewis Flight Propulsion Laboratory
Cleveland, Ohio

Classification cancelled (or changed to Unclassified)
NASA Tech Pub Announcement # 3
(AUTHORITY TO CHANGE)
4 Feb. 59
NIK

GRADE OF OFFICER MAKING CHANGE
15 Mar. 61
CLASSIFIED DOCUMENT
This material contains information affecting the National Defense of the United States within the meaning of the espionage laws, Title 18, U.S.C., Secs. 793 and 794, the transmission or revelation of which in any manner to an unauthorized person is prohibited by law.

NATIONAL ADVISORY COMMITTEE FOR AERONAUTICS

WASHINGTON
February 3, 1953

RECEIPT SIGNATURE

~~CONFIDENTIAL~~

319.98/13



MI

NACA RM E52L02

~~CONFIDENTIAL~~

NATIONAL ADVISORY COMMITTEE FOR AERONAUTICS

RESEARCH MEMORANDUMFREE-FLIGHT PERFORMANCE OF A ROCKET-BOOSTED, AIR-LAUNCHED
16-INCH-DIAMETER RAM-JET ENGINE AT MACH NUMBERS UP TO 2.20

By John H. Disher, Robert C. Kohl, and Merle L. Jones

SUMMARY

The investigation of air-launched ram-jet engines has been extended to include a study of models with a nominal design free-stream Mach number of 2.40. These models require auxiliary thrust in order to attain a flight speed at which the ram jet becomes self-accelerating. A rocket-boosting technique for providing this auxiliary thrust is described and time histories of two rocket-boosted ram-jet flights are presented. In one flight, the model attained a maximum Mach number of 2.20 before a fuel system failure resulted in the destruction of the engine. Performance data for this model are presented in terms of thrust and drag coefficients, diffuser pressure recovery, mass-flow ratio, combustion efficiency, specific fuel consumption, and over-all engine efficiency.

INTRODUCTION

As part of an extensive program concerned with the study of ram-jet engines, the NACA Lewis laboratory is investigating a series of 16-inch-diameter ram jets by launching these fin-stabilized, unguided engines from a carrier plane at high altitude. During descent, performance data are obtained by means of telemetering and radar.

The initial series of engines, designated types A, B, C, and D, had single oblique-shock-type inlets and were designed for oblique shock interception with the diffuser lip at a free-stream Mach number of 1.8. These engines, which had margins of thrust over drag in the transonic Mach number range, were capable of self-acceleration from subsonic to supersonic speeds. Results of these investigations are described in references 1 to 7. Upon completion of the investigation of these engines, plans were made to extend the Mach number range of the investigation. A fixed-geometry engine with a double oblique-shock-type diffuser and a design free-stream Mach number of 2.4 was selected for this phase of the program. This ram-jet engine has been designated type F. Calculation of off-design performance of this engine indicated that the

~~CONFIDENTIAL~~

2752

engine was incapable of self-acceleration through the transonic Mach number range and therefore rocket boost would be required for acceleration from the subsonic launching speed to an acceptable supersonic take-over speed for the ram jet. While the type F engine was being built, preliminary evaluations of a boosting technique were made by using type C engines, which were available.

Results of these preliminary evaluations of the boosting technique and results of a subsequent flight of the type F engine are described herein. Data are presented on diffuser pressure recovery, external drag, thrust coefficient, combustion efficiency, specific fuel consumption, and engine efficiency for the type F engine at Mach numbers from 1.5 to 2.19 and mass-flow ratios of 0.65 to 0.99. Ram-jet performance of the C model is not included inasmuch as reference 5 presents similar data.

APPARATUS

A sketch of the type C engine with rocket is shown in figure 1 and a detailed description of the engine is presented in reference 5. A photograph of the type F engine mounted on the carrier airplane is shown in figure 2. A sketch of the type F engine with rocket is shown in figure 3. The diffuser is of the double oblique-shock type with no internal contraction and with cone half-angles of 22° and 35° . The cowl lip is positioned to intercept the oblique shocks at a flight Mach number of 2.4. In order to obtain the maximum thrust in the lower Mach number range, a straight pipe exit was used. With this straight pipe, the engine was designed to operate critically with a $\mu^2\tau$ (where μ is equal to 1 plus the fuel-air ratio and τ is the ratio of exit total temperature to inlet total temperature) of approximately 3.6 at a Mach number of 2.0. This value of $\mu^2\tau$ corresponds to a burned fuel-air ratio of about 0.030 at 12,000 feet altitude and gives a combustor-inlet Mach number in front of the flame holder of approximately 0.23. Structural tolerances in building the engine altered these figures somewhat so that the actual critical values of $\mu^2\tau$ and of combustion-chamber-inlet Mach number approximate 3.3 and 0.240, respectively.

The booster rockets used were the 14-AS-1000 and the 6-KS-3000, T-40 solid propellant units. The 14-AS-1000 unit was used in the preliminary investigations while the 6-KS-3000 rocket was used for the F model. The 14-AS-1000 rocket produces 1000 pounds of thrust for 14 seconds and weighs approximately 195 pounds; the 6-KS-3000 rocket is rated at 3000 pounds of thrust for 6 seconds at sea level and weighs 133 pounds. The rockets were mounted within the combustion chamber on rollers and were retained in the engine by a shear pin. With the rockets mounted internally, a smaller shift in the center of gravity of the booster - ram jet combination was obtained than would be obtained with external

mounting, and the need for large booster fins was eliminated. Electric heating blankets and insulation were carried within the sheet metal rocket housing for temperature control of the rocket grain.

The rockets were ignited by 5-second delay squibs which were fired by a trailing line as the engine left the airplane. The rocket thrust sheared the retaining pin and after burnout, the rocket was ejected by drag forces. In order to obtain an adequate separation force, a wooden drag ring, shown in figure 3, was attached to the rocket housing. A lanyard attached to the ejected rocket triggered the fuel release and closed the flare ignition switch. Stabilizing fins attached to the rocket housing guided the ejected rocket on a predictable trajectory.

The thrust of the 14-AS-1000 rocket was transmitted to the ram-jet structure through the flame holder, whereas four bearing pads attached to the ram-jet shell were used to transmit the thrust of the 6-KS-3000 rocket.

To restrict the combustor-inlet velocity during ram-jet ignition, an aluminum "burnout" plate was attached at the ram-jet outlet by means of readily melted aluminum links. The plate was cut out to provide clearance for the rocket rollers, as shown in figure 4. The star-type flame holder (fig. 5) carried 12 magnesium flares for ignition purposes. The flares had a burning time about equal to that of the ram jet in order to ensure reignition of the engine following any in-flight blow-out that might occur. The combined heat release rate of the twelve flares was constant at 2600 Btu per second, which constituted 13 percent of the total heat release during ram-jet starting when the fuel flow was low. At the end of the flight the flares were providing only 2 percent of the total heat release. The projected blocked area of the flame holder is 57 percent of combustor cross-sectional area. At a combustion-chamber-inlet Mach number of 0.24, the total-pressure loss across the flame holder - spray ring combination was equal to about 2.7 times the combustion-chamber-inlet dynamic pressure.

The fuel system of the F model (fig. 6) differed considerably from the previous design described in reference 5; however, the basic principle of operation remained the same. Helium stored at high pressure was used for expelling fuel and the helium pressure was regulated to give a fuel flow rate nearly proportional to free-stream total pressure. A major change was the use of a cast aluminum piston and cylinder-type fuel tank with a 10.5-gallon capacity in place of the bladder type. This change was made in order to eliminate occasional fuel cell failure. The helium storage reservoir was changed from a helical tube to a spherically ended cylinder. Several modifications were made in the fuel regulation system: An initial stage of helium pressure regulation was incorporated to reduce the helium tank pressure to 800 pounds per square

inch at the inlet to the fuel-pressure regulator, whereas formerly the fuel-pressure regulator was subjected to the helium storage pressure. This change, which reduced the impact loads in the regulator valve at starting conditions, increased reliability and also improved regulation sensitivity at low rates of fuel flow. A bleed-off port was provided to allow regulated pressure to decrease rapidly if so required. In order to prevent excessive fuel flow during a combustion blow-out, an additional diaphragm was added to the regulator to correct the fuel pressure for variations in combustion-chamber-inlet static pressure, thus making the fuel pressure differential across the nozzles proportionate to free-stream total pressure. Formerly, the nozzle differential pressure varied with both free-stream total and combustion-chamber-inlet static pressures. Spring loaded, variable-area-type fuel nozzles were used for both engines reported herein rather than the fixed-orifice type previously used. Fuel used throughout the tests was unleaded aviation gasoline.

The weight of the engine-booster combination at release was 711 pounds and the weight of the engine at ram-jet ignition was 536 pounds.

INSTRUMENTATION

A radar-tracking unit, type SCR-584, with optical tracking facilities was used to determine the position of the model in space at approximately 0.1-second time intervals. Velocities of the winds aloft are obtained by radar tracking a weather balloon which is released immediately after the missile drop.

The C model engine carried an eight-channel telemetering transmitter similar to that described in reference 2. The F model carried a ten-channel telemetering transmitter with two switched channels allowing 12 measurements (see fig. 3) to be made. Acceleration was measured by use of two accelerometers, one measuring acceleration (-1 to 13 g's) and the other measuring deceleration (0 to -10 g's).

The fuel flow was determined from the pressure differential across a calibrated venturi. The venturi replaced the orifice used in the fuel measuring system of the C models. In order to measure accurately the wide range of fuel flow, two measurements were made of venturi differential pressure - one with a low range capsule (0 to 5 lb/sq in. differential) and the other with a high range capsule (0 to 50 lb/sq in. differential). The total pressures at stations 2 and 3 were measured by tapered-slot type averaging total-pressure probes of the kind described in reference 7. Total pressure at the engine outlet was measured by a copper-cooled rake, as shown in figure 7. The rake was

~~CONFIDENTIAL~~

constructed of Inconel with a copper core. The projecting tubes were made of molybdenum disilicide. When the rake is immersed in a high-temperature stream, the copper absorbs the heat transferred to the outer Inconel tube and maintains the rake at a safe temperature for the short time required.

CALCULATION PROCEDURE

The velocity and the free-stream Mach number of the engines during flight were calculated from telemetered total and static pressures and by integrating the total acceleration. The usual comparison of the velocity based on the telemeter records with that obtained from the radar data could not be made for these two flights because of incomplete radar records. Integrated acceleration is corrected for wind velocity.

Ambient-air temperature was obtained from an atmospheric survey made by the launching airplane immediately after the completion of the ram-jet drop.

Air flow through the engine was calculated from the static and dynamic pressure data at station 2 using a total temperature which was assumed equal to free-stream total temperature. The flow conditions at the diffuser exit (station 3) were then calculated from one-dimensional flow theory. The area at the diffuser exit is considered equal to the entire cross-sectional area of the combustion chamber. The total pressure, however, for convenience is measured in the annular area just ahead of the fuel spray ring. The total-pressure drop across the fuel spray ring and flame holder was determined from calibration runs made with no combustion, and this pressure drop was used to calculate the flow conditions immediately downstream of the flame holder (station 4). Thus the flow conditions presented for station 3 are based on a flow area of 1.4 square feet and the total pressure ahead of the fuel ring. The computed flow conditions just before combustion (station 4), although based on the same flow area (1.4 sq ft), take into account the pressure loss across the fuel spray ring and flame holder combination. Because the injected fuel is assumed still to be in the liquid state, the effect of fuel mass flow is not included in the flow computations for station 4.

The flow conditions after combustion were calculated using the continuity expression for mass flow. With choking at the exit, the exit Mach number at station 7 is assumed equal to 1.0, and the mass flow is equal to the computed air flow at station 2 plus the fuel flow. The measured total pressure at station 7 and an assumed specific heat ratio γ are used in the continuity expression to solve for an exit static temperature. The process is repeated until the assumed γ is that which corresponds to the computed temperature.

~~CONFIDENTIAL~~

Net thrust was calculated as the difference in the momentum of the exhaust gases at the engine outlet and the momentum of the free-stream air. External drag was determined as the difference between the net thrust and the product of the net acceleration times the instantaneous mass of the engine. Thrust and external-drag coefficients were calculated on the basis of the maximum cross-sectional area of 1.4 square feet.

Mass-flow ratio or capture area ratio was calculated as the ratio of actual internal air flow to the air flow in a free-stream tube having a diameter equal to that of the inlet lip. Maximum possible mass-flow ratio or β was calculated from cone flow theory.

Combustion efficiency η_c was determined as the increase in enthalpy of the fuel-air mixture across the combustion chamber divided by the available chemical energy of the fuel and flares.

The diffuser pressure recovery at stations 2 and 3 was calculated as the ratio of the observed total pressure in the diffuser to the calculated isentropic total pressure P_0 corresponding to the observed ambient pressure and free-stream Mach number.

The specific fuel consumption, defined as the rate of fuel flow in pounds per hour divided by pounds of thrust, was calculated on the basis of net thrust (designated TSFC) and also on the basis of propulsive thrust or thrust minus drag (designated PSFC).

The engine efficiency parameter η_e/η_c is defined as power output divided by power input, corrected to 100 percent combustion efficiency,

$$\frac{\eta_e}{\eta_c} = \frac{(T-D)V_0}{\eta_c(W_f h + H)778}$$

where

- (T-D) thrust minus drag (or propulsive thrust), lb
 V_0 free-stream velocity, ft/sec
 η_e engine efficiency
 η_c combustion efficiency
 W_f fuel flow, lb/sec
 h heating value of fuel, Btu/lb

H heat release rate of flares, Btu/sec
778 mechanical equivalent of heat, ft-lb/Btu

The remaining equations used in these calculations are presented in reference 2.

RESULTS AND DISCUSSION

Booster Separation and Ram-Jet Ignition

Time histories of the booster separation to ram-jet ignition phase of the two flights are shown in figure 8, which presents Mach number, acceleration, and fuel flow against time. Figure 8(a) for the C engine shows that the engine was boosted to a Mach number of 1.23 within 19 seconds after release. Rocket burnout is indicated by the abrupt drop in acceleration. Completion of rocket separation, fuel release, and ram-jet ignition are indicated by the increase in acceleration at 20 seconds; intermittent burning takes place until 21.9 seconds when the exit flow restrictor burns out, causing a momentary blow-out followed by normal operation at 23 seconds. Part (b) of figure 8 shows that the F engine was boosted to a Mach number of almost 1.55 within 12.7 seconds after release, and that 3.8 seconds were required for rocket separation, fuel release, and steady ram-jet ignition. Separation and fuel release occurred at 13 seconds and steady ram-jet combustion started at 16.5 seconds. The ejection of the exit restrictor takes place at 18.1 seconds and within 0.2 second the associated increase in thrust is evidenced by a rise in acceleration at 18.3 seconds.

Complete flight histories of free-stream Mach number, acceleration, and altitude against time for the two engines are shown in figure 9. The C engine accelerated to a maximum Mach number of 1.59 within 28.4 seconds after release. At that point the combustor blew out because of an excessively rich fuel-air ratio. The acceleration reached a peak value of 2.5 g's just before blow-out. The F engine had reached an altitude of 18,000 feet at 26 seconds and had accelerated to a maximum Mach number of 2.20 when the engine was destroyed by an explosion, which is thought to have resulted from a structural failure in the fuel system. The maximum acceleration attained during booster operation was 6.9 g's and during the ram-jet operation, 5.7 g's.

Engine Performance

Inasmuch as the performance of the C model is similar to that presented in reference 5, the performance data for this engine are not presented herein. Time histories of the important variables for the

F model are presented in figure 10. This figure has been arranged in parts (a) to (c) describing free-stream conditions, diffuser and combustor conditions, and basic performance parameters, respectively.

In figure 10(a), it can be seen that the Reynolds number (based on body length) varied from 22,000,000 to 154,000,000 during the flight and that the free-stream total temperature and pressure reached maximum values of 904° R and 12,000 pounds per square foot absolute, respectively.

The total pressure measured at stations 2, 3, and 7, the static pressure, temperature, velocity, and Mach number calculated for station 3, and the fuel flow are shown in figure 10(b). The basic engine performance parameters of thrust coefficient, thrust minus drag coefficient, total-temperature ratio, fuel-air ratio, and combustion efficiency are presented in figure 10(c). The combustion efficiency attained a maximum value of only 61 percent before the sudden enrichment brought on by the spray ring failure near the end of the flight caused the efficiency to decline rapidly. Factors which probably contribute to the comparatively low combustion efficiency throughout the flight include the low initial temperature of the fuel and the uniform type fuel distribution pattern, which forestalls rich blow-out by eliminating regions of excessive fuel concentration at rich mixtures but does not provide for efficient operation in the lean range.

These time histories provide a convenient method of presenting the basic information on the flight performance of this engine as well as of indicating the rate of change of the variables. However, for purposes of analysis, the important parameters are plotted against free-stream Mach number.

Diffuser Pressure Recovery

The pressure recovery data as measured at stations 2 and 3 are shown in figure 11. Values of combustion-chamber-inlet Mach number M_3 are indicated for each data point and a line representing approximately critical M_3 is faired through the data. Near critical operation was obtained in the Mach number range from 1.57 to 2.10, during which time the diffuser pressure recovery decreased from 0.92 to 0.88. The theoretical shock recovery for the diffuser is shown by a dashed line. It is interesting that with critical operation, the theoretical recovery of 0.93 is approached at station 2 for M_0 of 2.1. This high recovery indicates that the friction loss from the inlet to station 2 (approximately 27 in.) is negligible and that structural tolerances and finish imperfections of this sheet metal flight model have not adversely affected diffuser recovery. The recovery at station 3 indicates a friction loss of about 0.05 between stations 2 and 3 under critical operating

~~CONFIDENTIAL~~

conditions at M_0 of 2.1. At M_0 of approximately 2.1, the heat addition decreased, allowing the diffuser to operate supercritically. The drop in pressure recovery above $M_0 = 2.10$ reflects these supercritical losses.

Thrust Coefficient

For an engine of fixed geometry at zero angle of attack, the thrust coefficient C_F is primarily a function of M_0 and $\mu^2\tau$. The thrust coefficient is plotted against M_0 in figure 12 with values of $\mu^2\tau$ indicated for each data point. The value of $\mu^2\tau$ up to M_0 of 2.10 is close to critical and a line representing this critical condition is faired through the data. With critical heat addition, the thrust coefficient increased from 0.56 at $M_0 = 1.57$ to 0.82 at $M_0 = 2.10$. At this point, the heat addition drops below critical and the thrust diminishes accordingly. The drop in heat addition is believed to have been caused by a structural failure in the fuel nozzle manifold which let an excessive amount of unatomized fuel into the combustor.

Drag Coefficient

With the thrust defined as momentum change of the internal air flow and fuel flow from free stream to engine outlet, the total external drag includes additive drag (see ref. 8 for definition of additive drag) as well as skin-friction drag and cowl-pressure drag. At a given M_0 the important variable affecting additive drag and cowl-pressure drag is mass-flow ratio m/m_0 ; therefore m/m_0 is plotted against M_0 in figure 13. Although the nominal design M_0 of the engine is 2.4, m/m_0 approaches 1.0 at M_0 of approximately 2.2. The discrepancy is due to structural tolerances in the fabrication of the engine, the actual inlet area being larger than the nominal design area. A convenient index of flow conditions for a given inlet configuration is the parameter $(m/m_0)(1/\beta)$, where β is the theoretical maximum attainable mass-flow ratio for that configuration at the given M_0 . Thus when $(m/m_0)(1/\beta)$ is approximately 1.0, the engine is operating critically or supercritically and values less than 1.0 would indicate subcritical operation. The total-external-drag coefficient is plotted against M_0 in figure 14 with values of $(m/m_0)(1/\beta)$ indicated for each data point. These values are approximately 1.0 throughout the flight, indicating near-critical or supercritical operation. The estimated friction-drag coefficient (based on the maximum cross-sectional area) is indicated by the dashed line on the drag curve. The vertical distance between the solid and dashed lines

~~CONFIDENTIAL~~

thus represents the sum of the cowl pressure and additive drags. The friction drag of the engine was obtained from reference 7, which presents skin-friction coefficients determined in flight for a C type engine. The data of reference 7 were extrapolated to the higher Mach number and Reynolds number attained in this flight by use of reference 9. The external wetted area of the F engine to which the skin-friction coefficients were applied was 76.6 square feet.

Inasmuch as the flow parameter $(m/m_0)(1/\beta)$ indicates that approximately maximum possible air flow is being taken into the engine throughout the flight, the additive drag is a minimum and this total-drag curve represents the minimum drag condition for this engine. Subcritical operation would increase the drag from the minimum values. Although the additive drag is at a minimum, it nevertheless makes up a major part of the total drag in the lower Mach number range because of the low mass-flow ratios indicated in figure 13. At M_0 of 1.57, the sum of the additive- and cowl-pressure-drag coefficients based on the estimated friction drag is approximately 0.21 or about two-thirds the total external-drag coefficient of 0.34; at M_0 of 2.10, the sum of the additive- and cowl-pressure-drag coefficients has diminished to approximately 0.07 or about 40 percent of the total external-drag coefficient of 0.18. With m/m_0 equal to 0.99 at M_0 of 2.17, the additive drag is approaching zero and the total-drag coefficient of 0.14 results primarily from friction and cowl-pressure drags. Based on the estimated friction drag, the cowl-pressure-drag coefficient is approximately 0.04 at M_0 of 2.17.

Propulsive Thrust Coefficient

The propulsive thrust coefficient, or thrust minus drag coefficient $(C_F - C_D)$, for a fixed-geometry engine at zero angle of attack is also primarily a function of M_0 and $\mu^2\tau$. The $(C_F - C_D)$ is plotted against M_0 in figure 15 with values of $\mu^2\tau$ again indicated for each data point; a line of critical $\mu^2\tau$ faired through the data rises from a $(C_F - C_D)$ of 0.22 at M_0 of 1.57 to a maximum of 0.64 at M_0 of 2.10. The steeper slope of the $(C_F - C_D)$ curve as compared with the C_F curve is due to a decreasing drag coefficient at the higher values of M_0 .

Specific Fuel Consumption

The thrust specific fuel consumption TSFC and propulsive thrust specific fuel consumption PSFC of the engine are presented in figure 16. In order to generalize the curves for comparison purposes, the

actual specific fuel consumptions have been multiplied by η_c so that the values shown correspond to 100 percent η_c . These fuel consumption parameters are plotted against M_0 and values of $\mu^2\tau$ are indicated for each data point. The fuel consumption is also shown in terms of specific impulse by use of the compound ordinate scale. Inasmuch as the specific impulse is an inverse function of the specific fuel consumption, the discussion of specific fuel consumption applies in an opposite sense to specific impulse.

With η_c eliminated as a variable, the TSFC of a fixed-geometry engine varies primarily with Mach number, free-stream static temperature t_0 , and $\mu^2\tau$. At constant M_0 and t_0 , the TSFC would be expected to decrease with $\mu^2\tau$ down to the critical value of $\mu^2\tau$, beyond which further reductions of $\mu^2\tau$ will result in an increase in TSFC. In the region of this minimum point, variations in $\mu^2\tau$, at constant M_0 and t_0 , will affect the TSFC only slightly. It is in this range that this engine is operating; therefore little variation from the critical curve is apparent for the supercritical operation at the end of the flight. The slight increase in TSFC with increasing M_0 above about 1.8 is the result of the falling diffuser pressure recovery and the increasing free-stream temperatures. As indicated in figure 10(a), the free-stream static temperature has increased from 420° to 454° R during the change in M_0 from 1.57 to 2.17. An over-all increase in the TSFC from the lower to the higher M_0 of 7.8 percent is observed; one-half this rise is attributed to temperature effect, the specific fuel consumption at constant M_0 and $\mu^2\tau$ being proportional to the square root of t_0 .

The PSFC of a fixed-geometry engine is much more sensitive to M_0 than the TSFC because of the adverse effects of off-design operation on drag. Because it is based on the net propulsive force produced by the engine, the PSFC is the more important factor. With M_0 varying from 1.57 to 2.17 and t_0 from 420° to 454° R, an over-all decrease in the PSFC (also corrected to 100 percent combustion efficiency) from 5.25 to 2.90 may be noted in figure 16(b). Correction to a temperature of 420° R would lower the PSFC at an M_0 of 2.17 to approximately 2.8. As would be expected under near critical operating conditions, the PSFC nears a minimum as the design M_0 is approached.

Engine Efficiency

A parameter reflecting the combined effects of the important variables on engine performance is engine efficiency. Analysis of the previously defined efficiency equation reveals that the important variables

affecting efficiency for a given engine are $\mu^2\tau$ and M_0 . The efficiency of this engine is therefore plotted against M_0 in figure 17 with values of $\mu^2\tau$ indicated for each data point. A line corresponding to approximately critical $\mu^2\tau$ is faired through the data. With approximately critical conditions the efficiency increases rapidly with increasing M_0 , rising from 0.07 at M_0 of 1.57 to 0.18 at M_0 of 2.10. With slightly supercritical operation, the efficiency reaches a maximum value of about 19 percent at M_0 of 2.17 and $\mu^2\tau$ of 2.90.

2752

SUMMARY OF RESULTS

Data obtained from the flight of a rocket-boosted, air-launched ram-jet engine with a nominal design free-stream Mach number of 2.40 provided the following results:

1. A satisfactory boosting technique has been developed in which the model is accelerated to supersonic speed by an auxiliary rocket, whereupon the engine is ignited and becomes capable of self-acceleration.

2. A maximum Mach number of 2.20 was achieved with steady combustion before a fuel system failure resulted in an explosion which destroyed the model while in flight.

3. Near critical operation was obtained in the Mach number range from 1.57 to 2.10, during which time the diffuser pressure recovery decreased from 0.92 to 0.88. A comparison with theoretical recovery across the oblique and normal shocks indicates a constant friction loss through the diffuser of about 5 percent. Supercritical operation was obtained from a Mach number of 2.1 to the end of the flight.

4. The increase in Mach number from 1.57 to 2.10 was accompanied by an increase in thrust coefficient from 0.56 to 0.82, while the external-drag coefficient diminished from 0.34 to 0.18. The corresponding rise in propulsive thrust coefficient was from 0.22 to 0.64.

5. Mass-flow ratios obtained closely paralleled the maximum theoretical values throughout the flight and had reached a value of 0.99 at a Mach number of 2.17. The external-drag coefficient at this near minimum additive-drag condition was 0.14.

6. The specific fuel consumption, based on propulsive thrust and corrected to a combustion efficiency of 1.00, reached a minimum of 2.90 at a Mach number of 2.17.

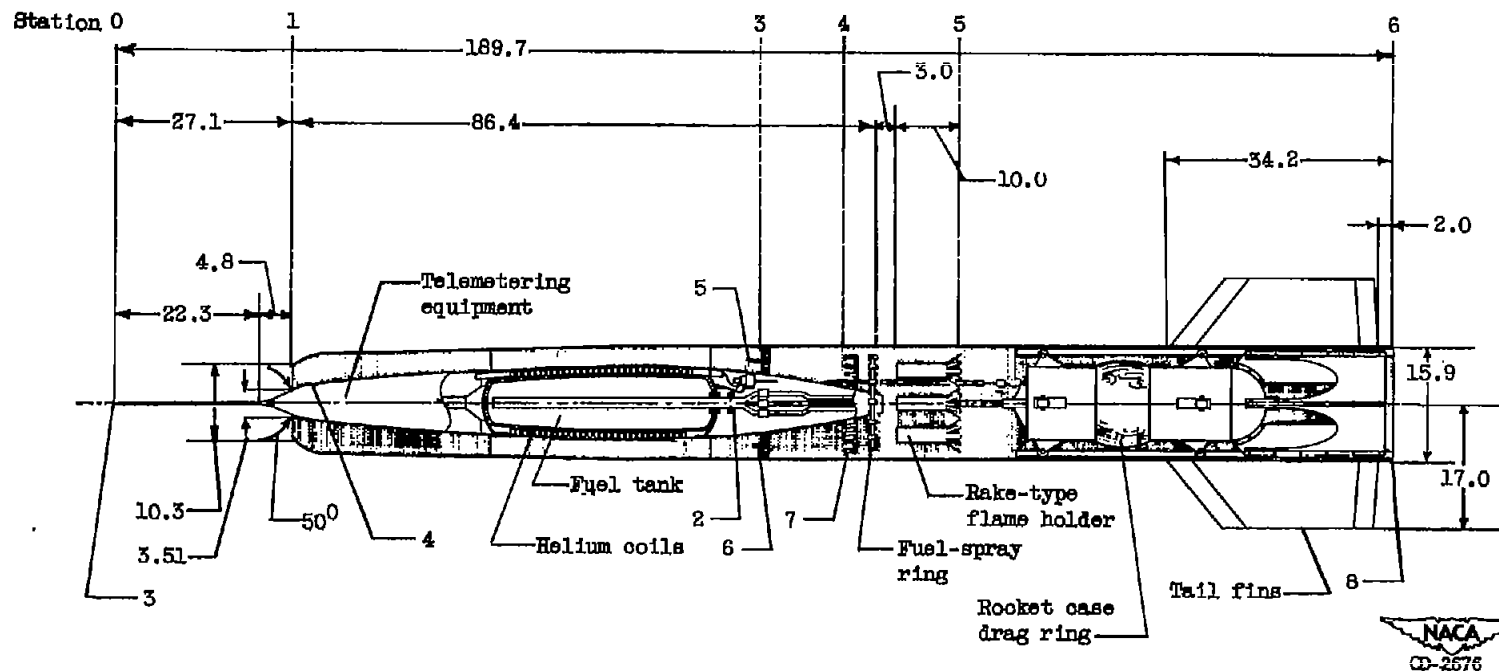
7. Over-all engine efficiency, when corrected to a combustion efficiency of 1.00, steadily increased from a value of 0.07 at a Mach number of 1.57 to 0.18 at a Mach number of 2.10.

Lewis Flight Propulsion Laboratory
National Advisory Committee for Aeronautics
Cleveland, Ohio

REFERENCES

1. Kinghorn, George F., and Disher, John H.: Free-Flight Investigation of 16-Inch-Diameter Supersonic Ram-Jet Unit. NACA RM E8A26, 1948.
2. Carlton, William W., and Messing, Wesley E.: Free-Flight Performance of 16-Inch-Diameter Supersonic Ram-Jet Units. I - Four Units Designed for Combustion-Chamber-Inlet Mach Number of 0.12 at Free-Stream Mach Number of 1.6 (Units A-2, A-3, A-4, and A-5). NACA RM E9F22, 1949.
3. Messing, Wesley E., and Simpkinson, Scott H.: Free-Flight Performance of 16-Inch-Diameter Supersonic Ram-Jet Units. II - Five Units Designed for Combustion-Chamber-Inlet Mach Number of 0.16 at Free-Stream Mach Number of 1.60 (Units B-1, B-2, B-3, B-4, and B-5). NACA RM E50B14, 1950.
4. Disher, John H., and Rabinowitz, Leonard: Free-Flight Performance of 16-Inch-Diameter Supersonic Ram-Jet Units. III - Four Units Designed for Combustion-Chamber-Inlet Mach Number of 0.245 at Free-Stream Mach Number of 1.8 (Units D-1, D-2, D-3, and D-4). NACA RM E50D07, 1950.
5. Rabb, Leonard, and North, Warren J.: Free-Flight Performance of 16-Inch-Diameter Supersonic Ram-Jet Units. IV - Performance of Ram-Jet Units Designed for Combustion-Chamber-Inlet Mach Number of 0.21 at Free-Stream Mach Number of 1.6 over a Range of Flight Conditions. NACA RM E50L18, 1951.
6. Messing, Wesley E., and Acker, Loren W.: Transonic Free-Flight Drag Results of Full-Scale Models of 16-Inch-Diameter Ram-Jet Engines. NACA RM E52B19, 1952.
7. Messing, Wesley E., and Rabb, Leonard: Transonic Free-Flight Investigation of the Total Drag and of the Component Drags (Cowl Pressure, Additive, Base, Friction, and Internal) Encountered by a 16-Inch-Diameter Ram-Jet Engine for Mach Numbers from 0.80 to 1.43. NACA RM E52F02, 1952.

8. Ferri, Antonio, and Nucci, Louis M.: Preliminary Investigation of a New Type of Supersonic Inlet. NACA TN 2286, 1951.
9. de Kármán, Th.: The Problem of Resistance in Compressible Fluids. Quinto Convegno "Volta," Reale Accademia D'Italia (Roma), Sett. 30-Ott. 6, 1935, pp. 3-57.



Instrument	Measurement
1	Axial net acceleration (not shown)
2	Fuel flow
3	Free-stream total pressure (behind normal shock)
4	Diffuser inlet static pressure

Instrument	Measurement
5	Static pressure in diffuser
6	Dynamic pressure in diffuser
7	Total pressure at combustion-chamber inlet
8	Static pressure at engine outlet

Figure 1. - Sketch of model C ram-jet engine showing major components, dimensions, and instrumentation. (All dimensions are in inches.)

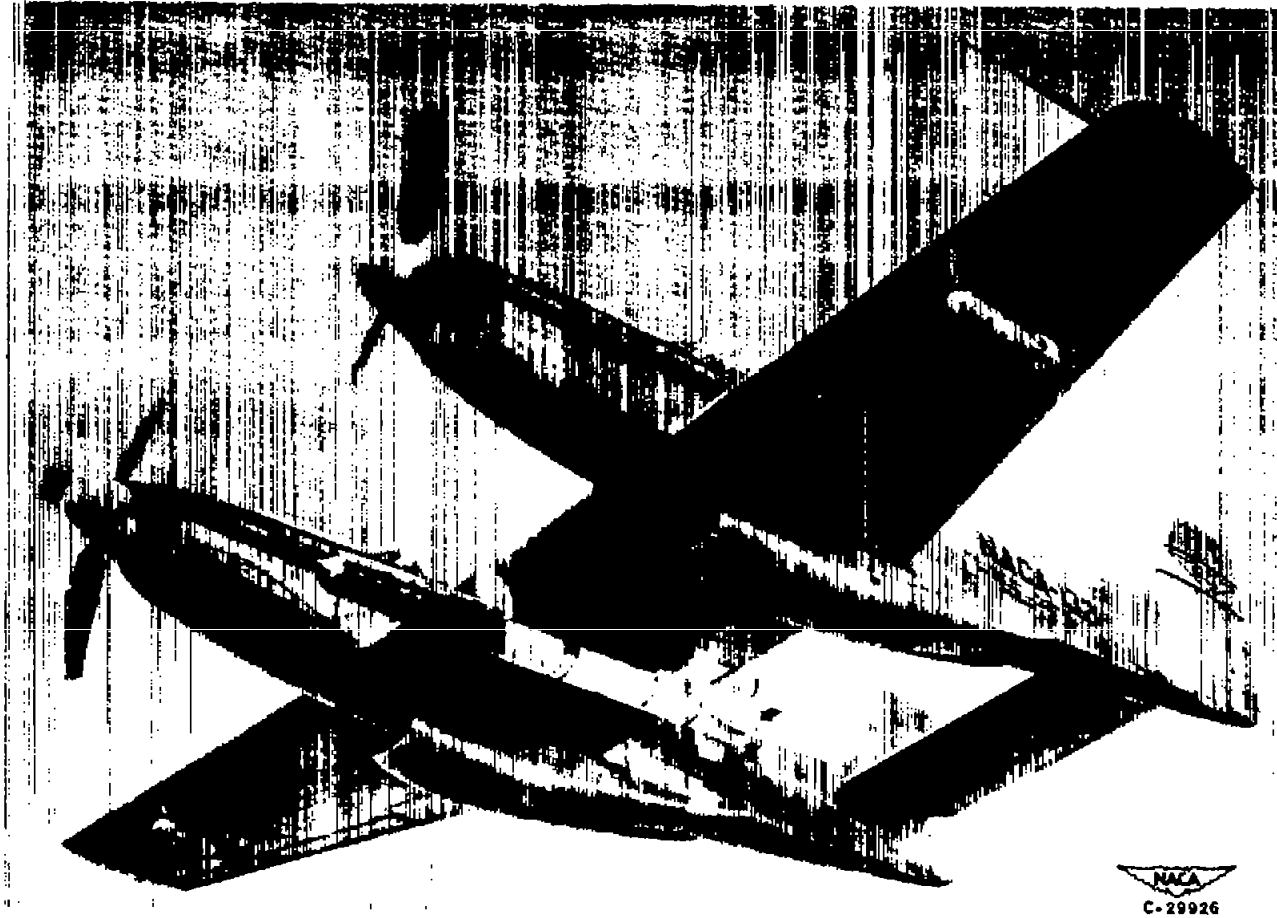
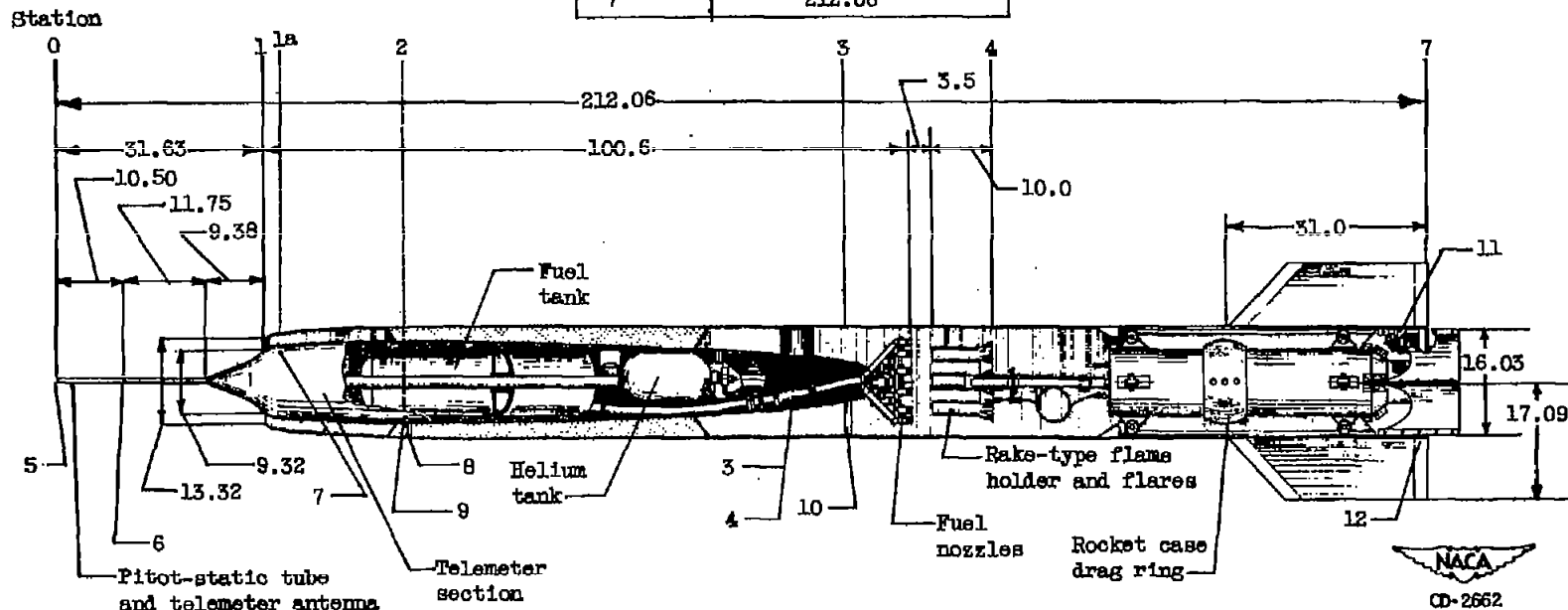


Figure 2. - Photograph of model F ram-jet engine mounted beneath central wing panel of carrier airplane.

Station	Distance from pitot-static tip, in.
1	31.63
1a	34.25
2	58.38
3	122.50
4	145.81
7	212.06



Instrument	Measurement
1	Axial net acceleration, positive (not shown)
2	Axial net acceleration, negative (not shown)
3	Fuel flow, low range
4	Fuel flow, high range
5	Free-stream total pressure (behind normal shock)
6	Free-stream static pressure

Instrument	Measurement
7	Static pressure in diffuser
8	Dynamic pressure in diffuser
9	Static pressure in diffuser
10	Total pressure in diffuser outlet
11	Total pressure at engine outlet
12	Static pressure at engine outlet

Figure 3. - Sketch of model F ram-jet engine showing major components, dimensions, and instrumentation. (All dimensions are in inches.)

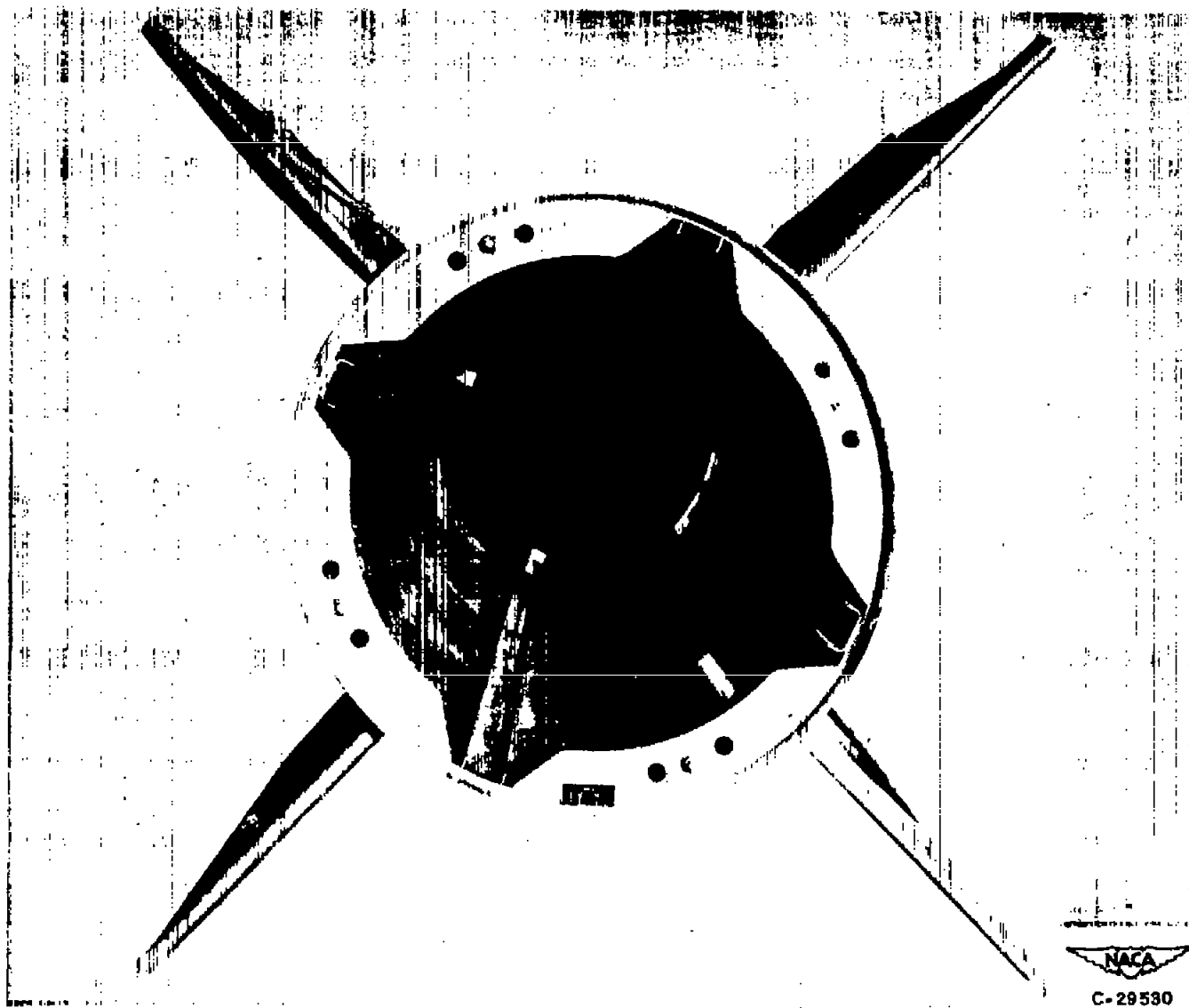


Figure 4. - Rear view of model F ram-jet engine showing burnout plate with rocket roller outouts.

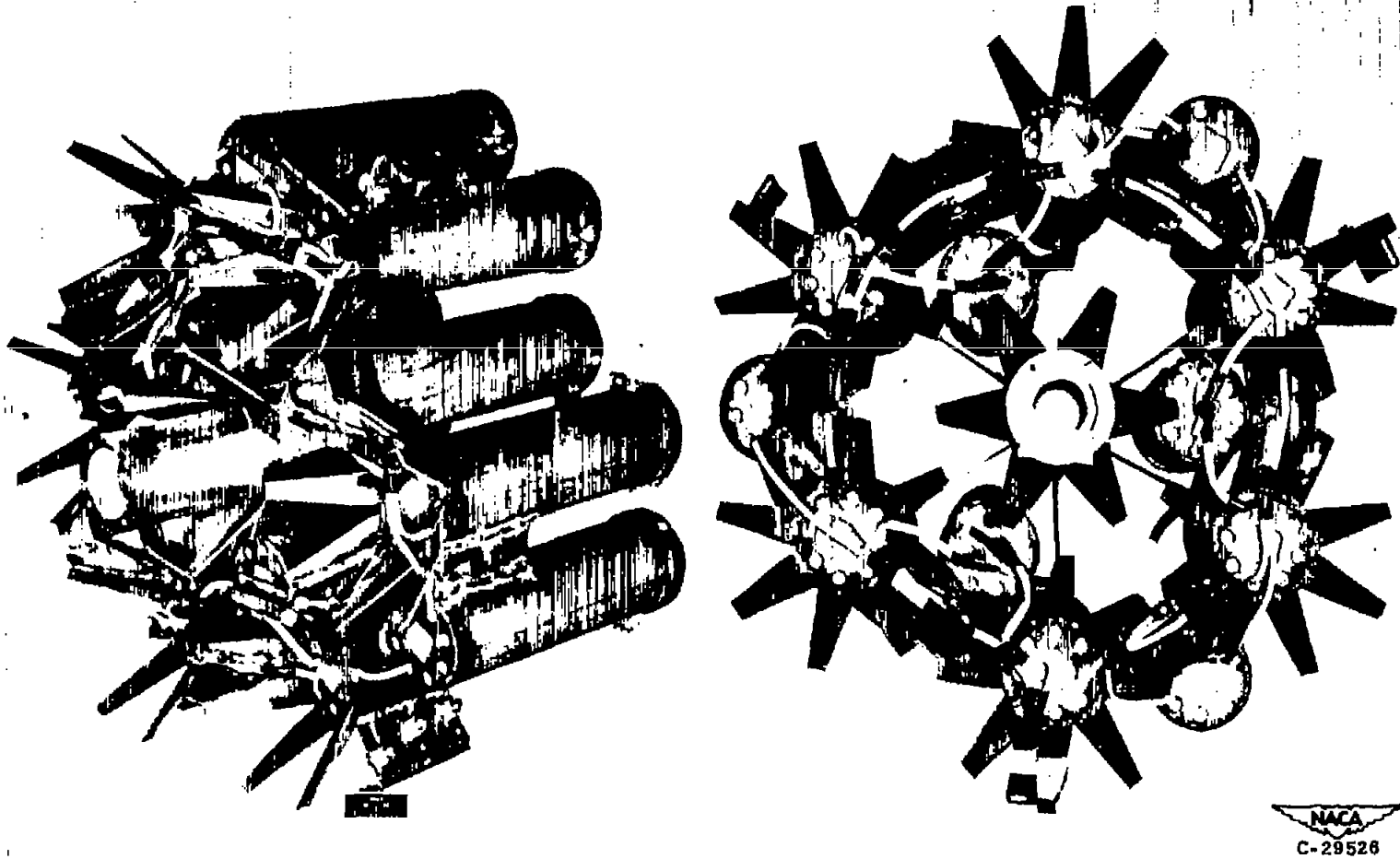


Figure 5. - Star-type flame holder and flare case combination used in model F ram-jet engines.

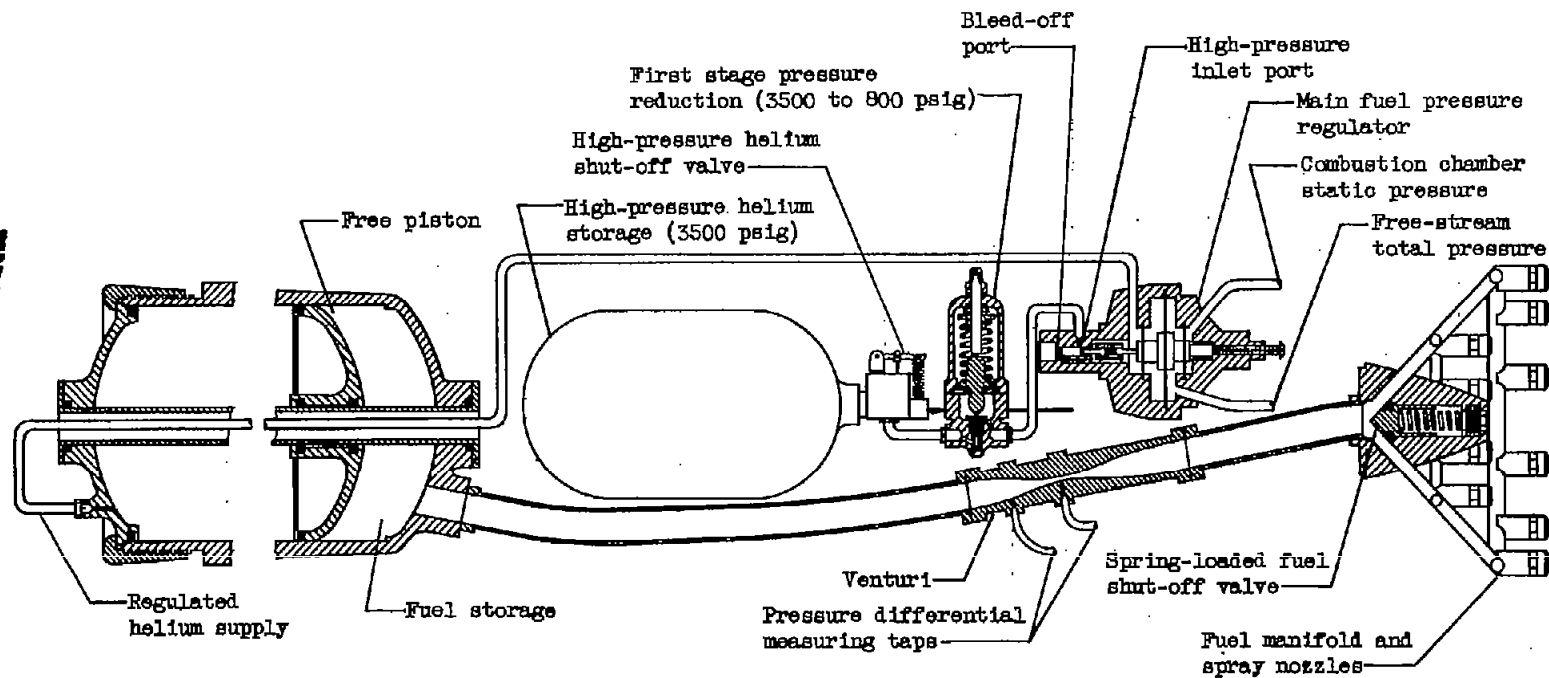


Figure 6. - Fuel system used in model F ram-jet engine.



CD-2802

CONFIDENTIAL

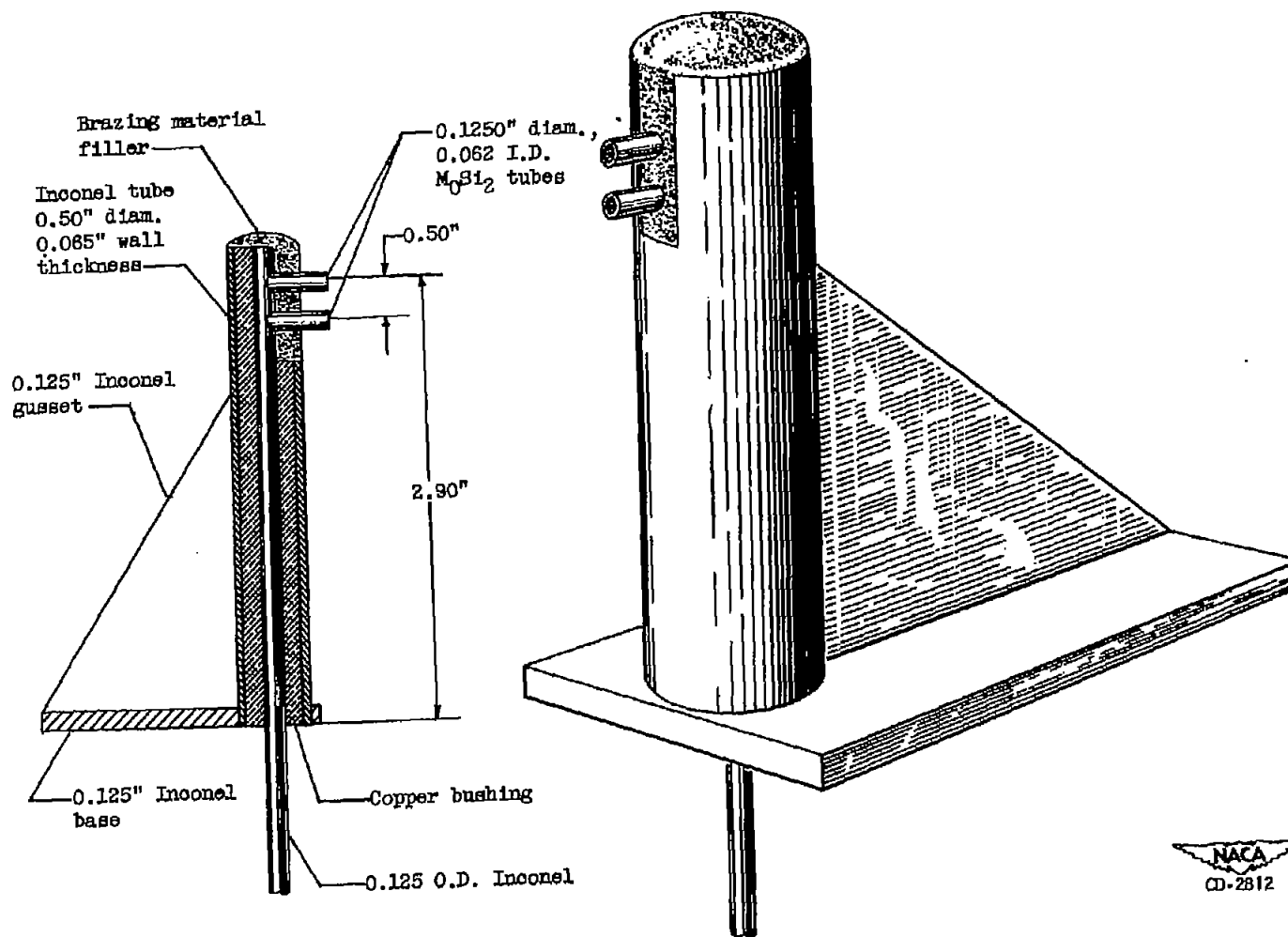


Figure 7. - Copper-cooled exit total-pressure rake construction detail.

IN CONSTRUCTION

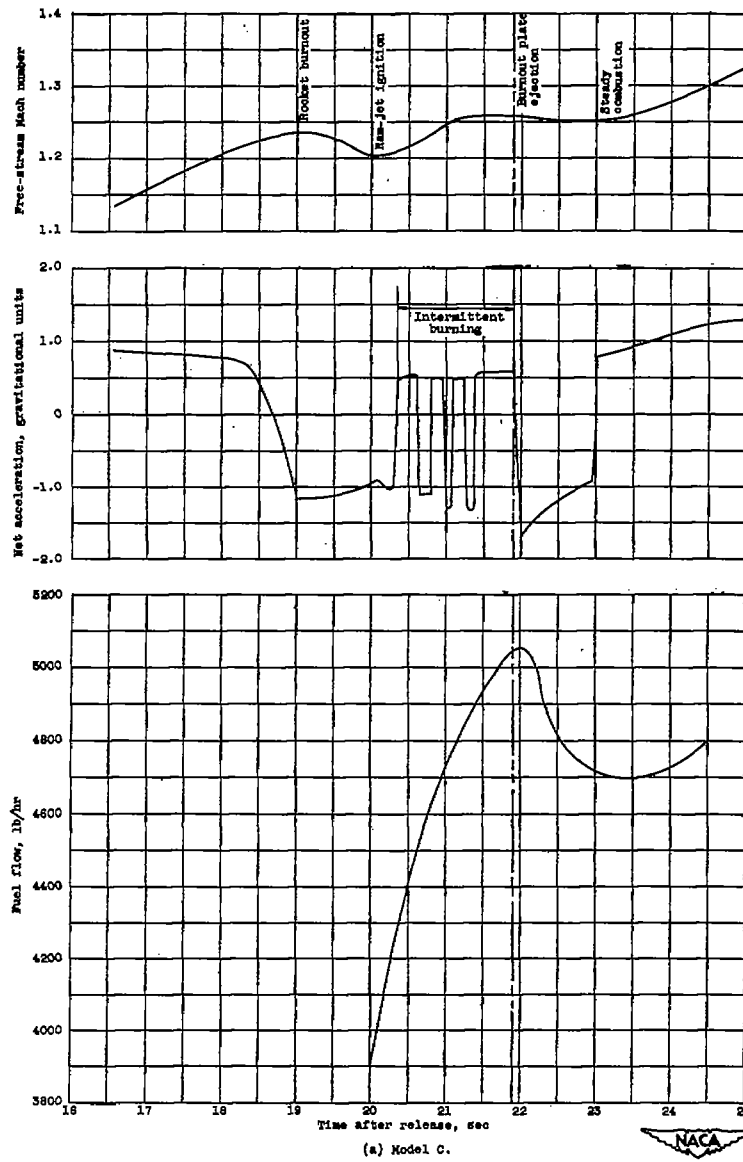


Figure 8. - Detailed time history of ram-jet engine, covering sequence from burnout of booster rocket to steady ram-jet combustion.

2752

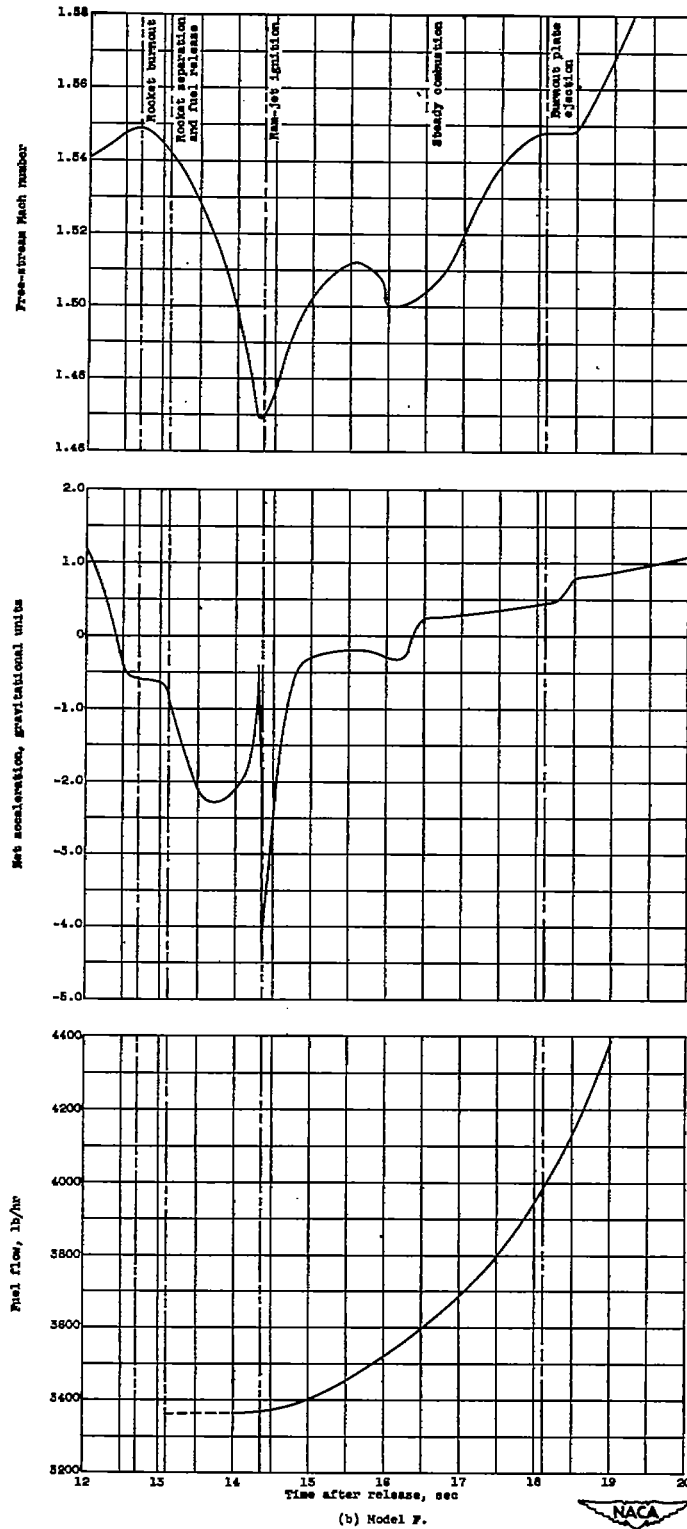


Figure 8. - Concluded. Detailed time history of ram-jet engine, covering sequence from burnout of booster rocket to steady ram-jet combustion.

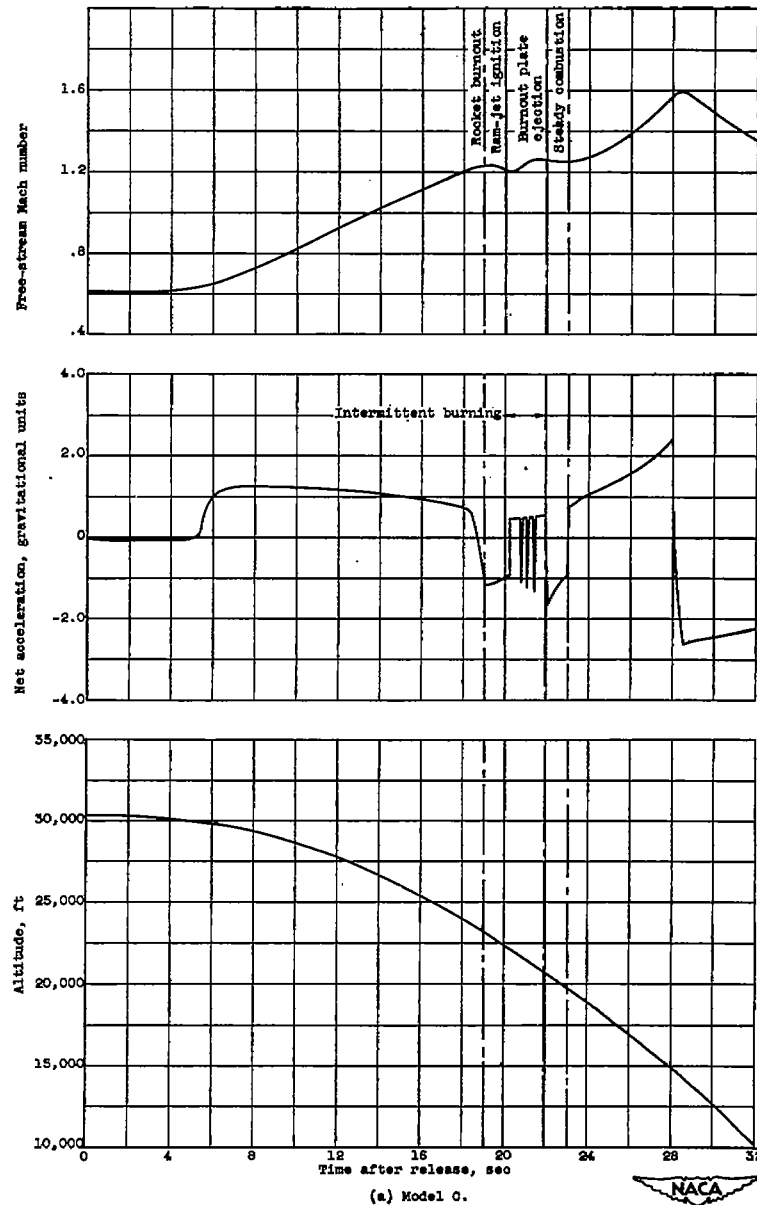
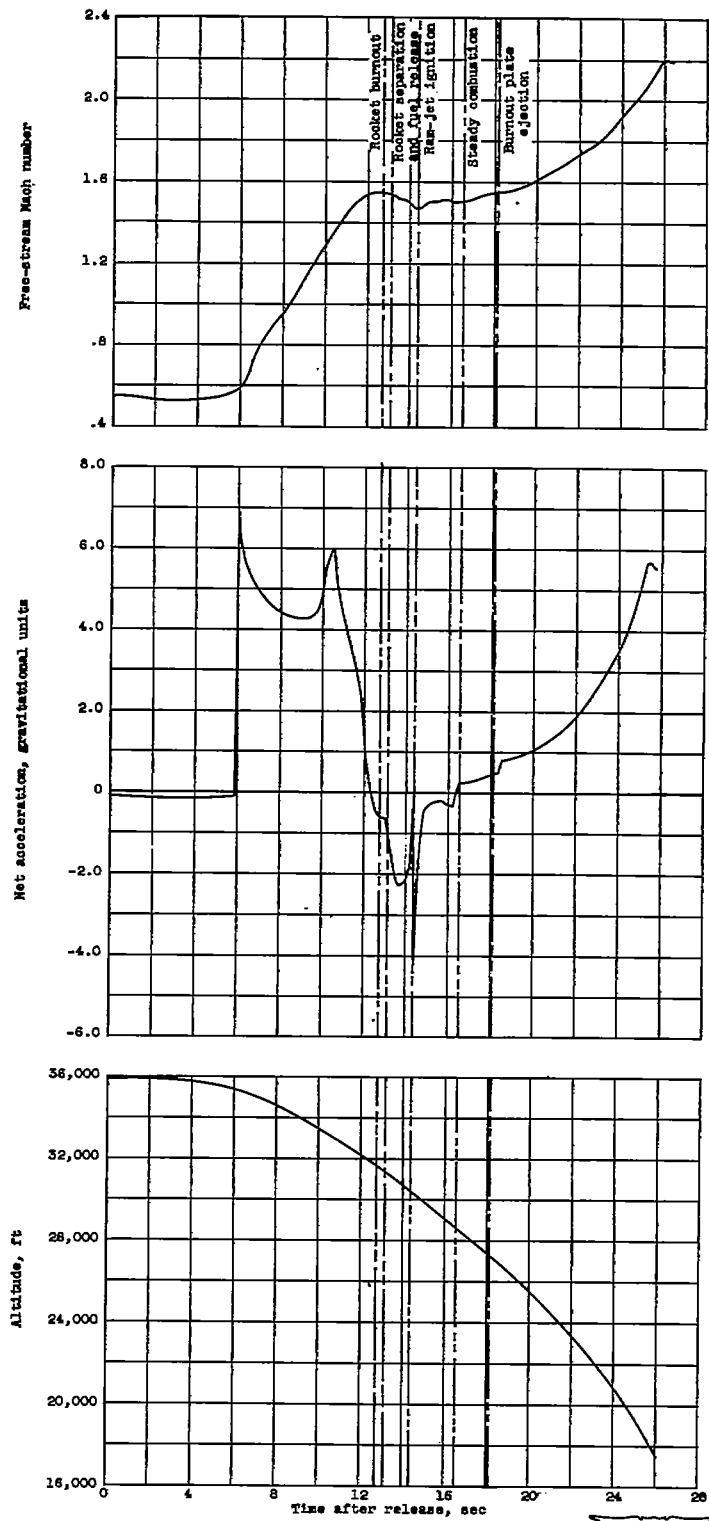


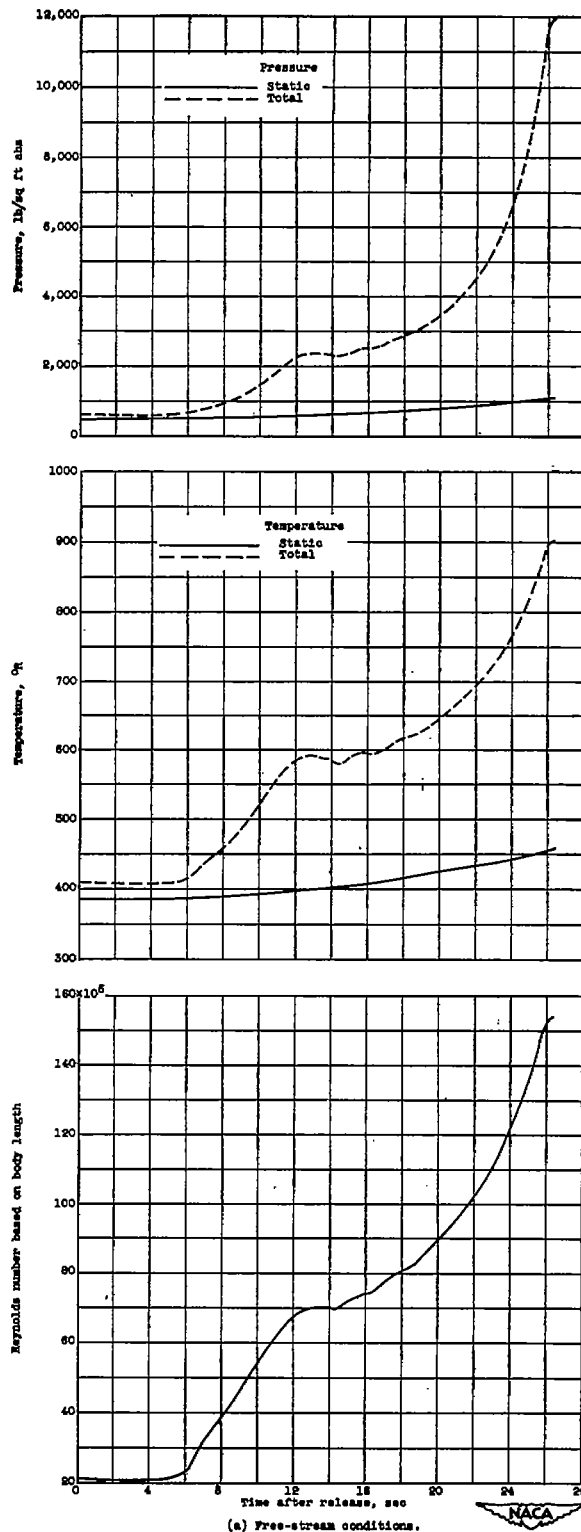
Figure 9. - Over-all time history of rocket-boostered ram-jet engine.



(b) Model F.

Figure 9. - Concluded. Over-all time history of rocket-boosted ram-jet engine.

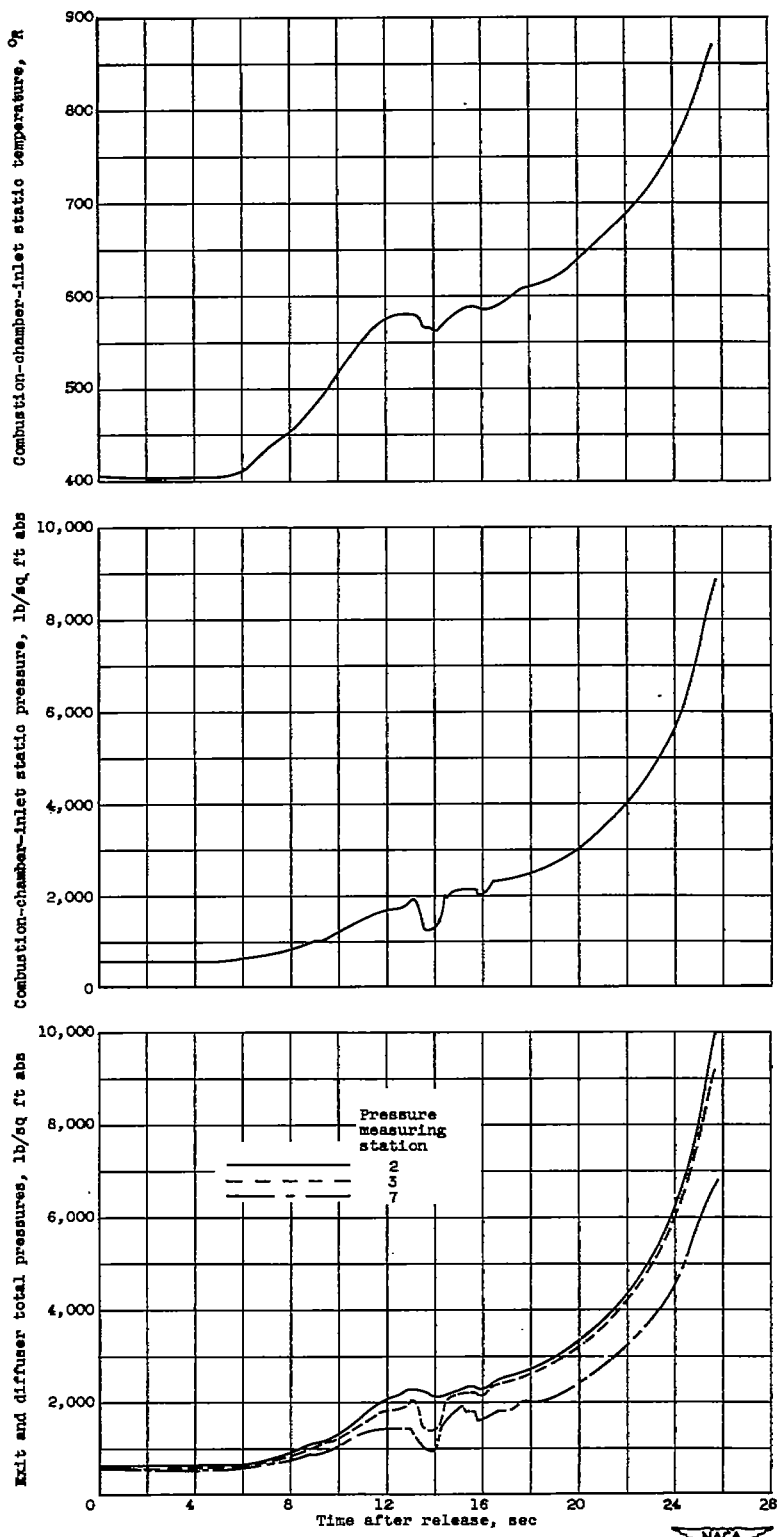




(a) Free-stream conditions.
 Figure 10. - Time histories of rocket-coated model F ram-jet engine.

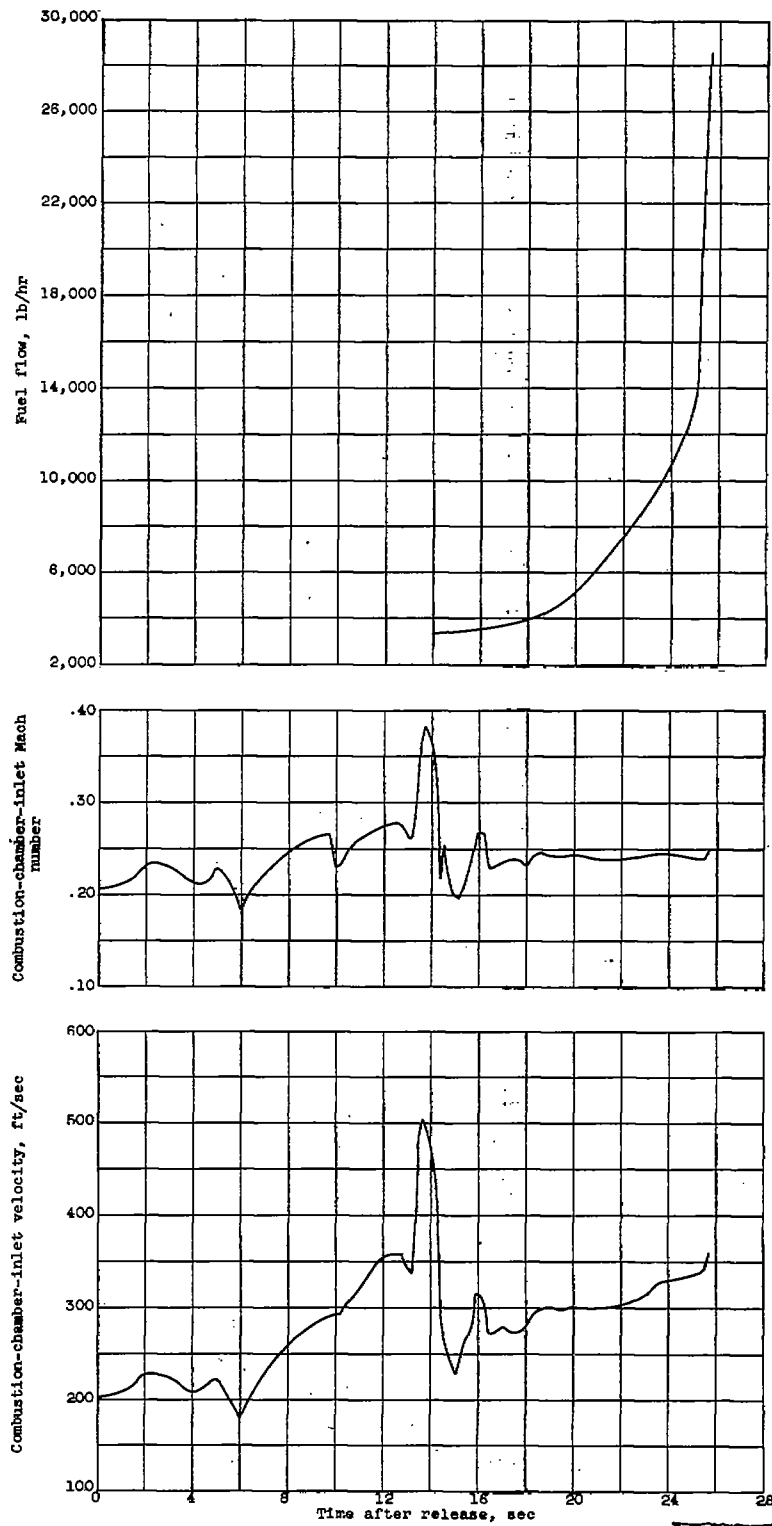
2752

2752



(b) Diffuser and combustor conditions.

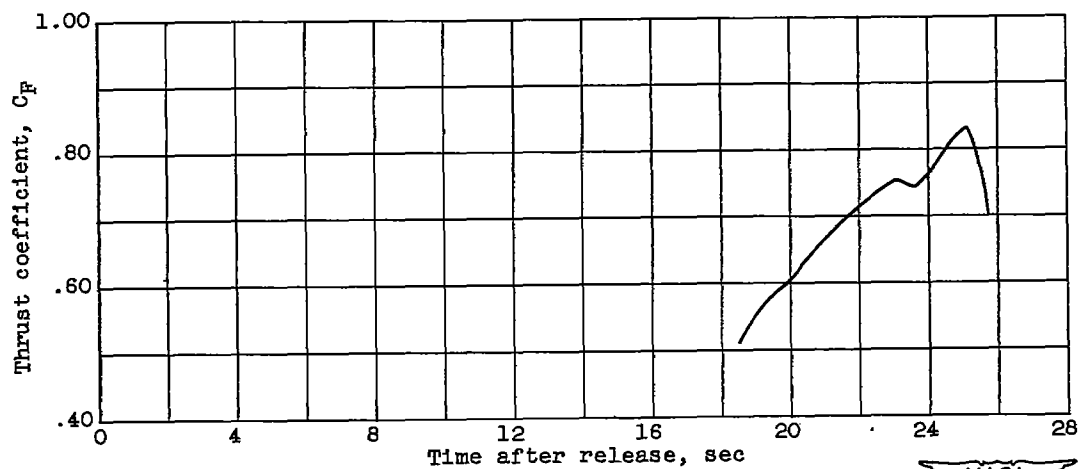
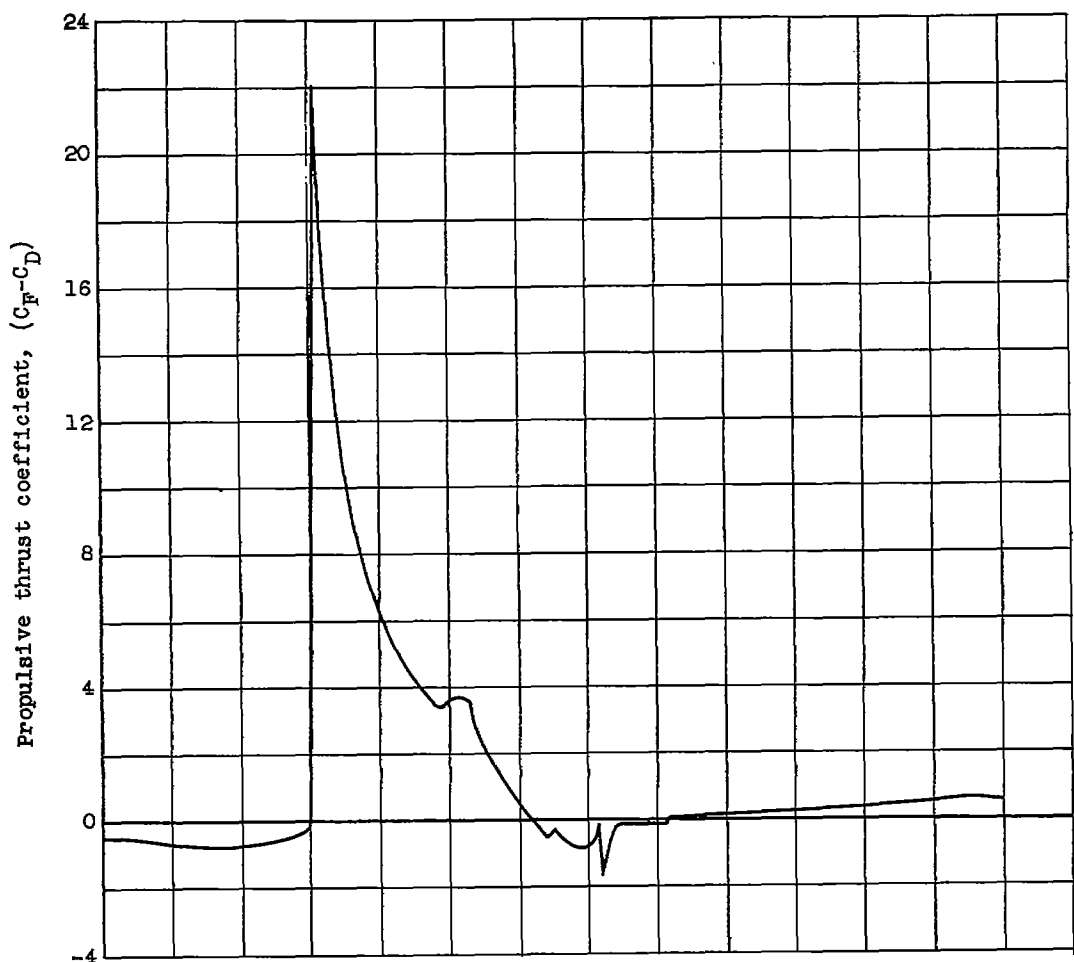
Figure 10. - Continued. Time histories of rocket-boosted model F ram-jet engine.



(b) Concluded. Diffuser and combustor conditions.

Figure 10. - Continued. Time histories of rocket-boosted model F ram-jet engine.

2752



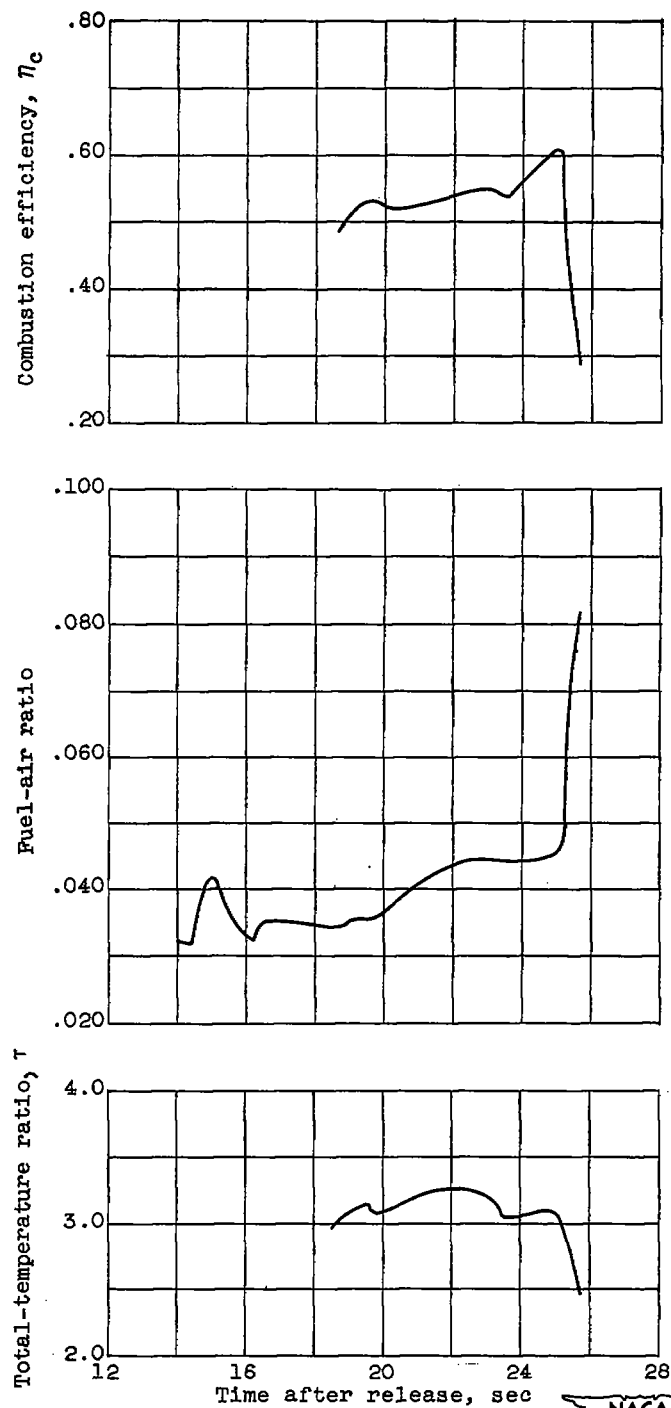
(c) Basic performance parameters.



Figure 10. - Continued. Time histories of rocket-boosted model F ram-jet engine.

2752

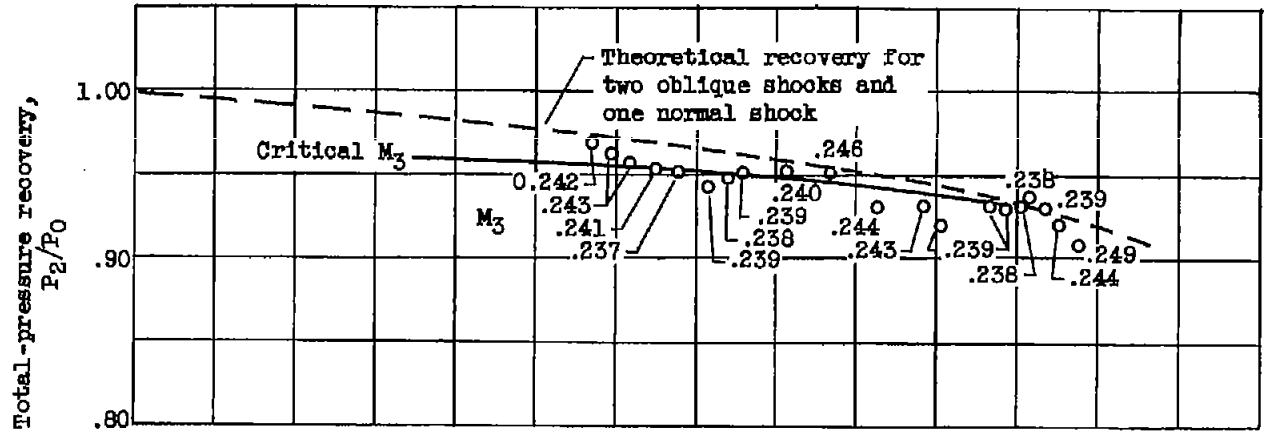
~~SECRET~~

~~CONFIDENTIAL~~

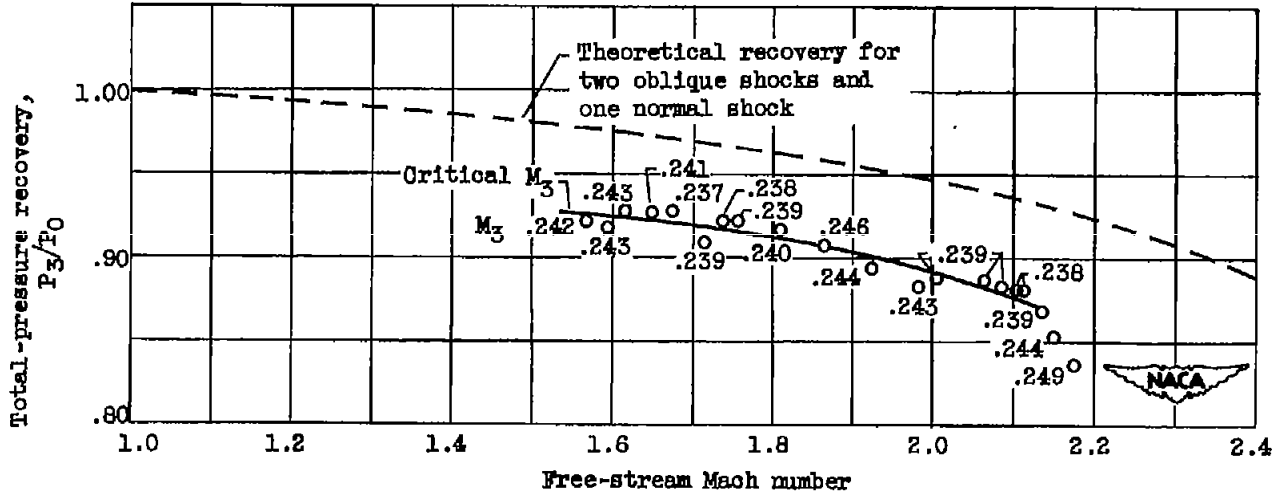
(c) Concluded. Basic performance parameters.

Figure 10. - Concluded. Time histories of rocket-boosted model F ram-jet engine.

~~CONFIDENTIAL~~



(a) At station 2.



(b) At station 3.

Figure 11. - Total-pressure recovery with indicated values of M_3 for model F ram-jet engine.

CONFIDENTIAL

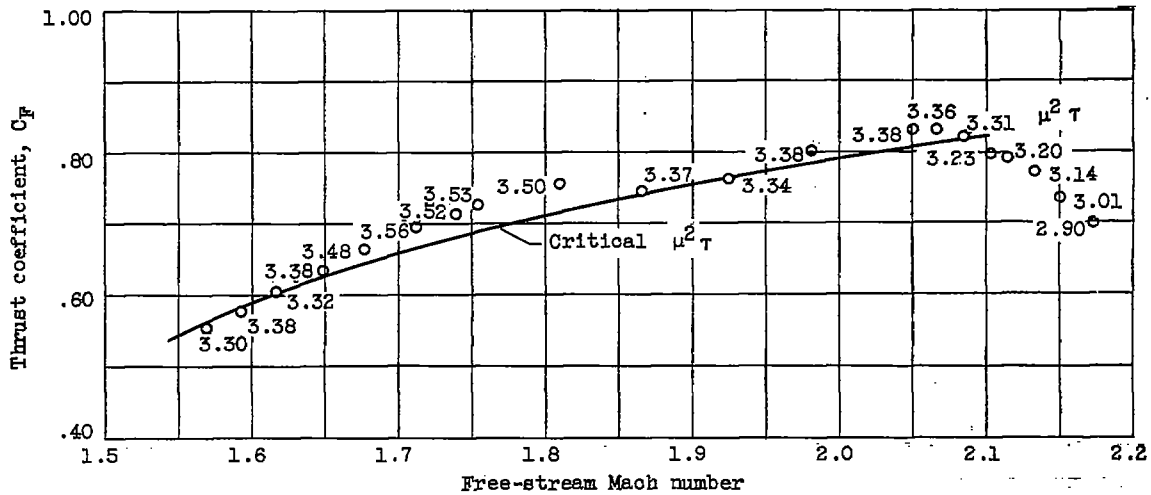


Figure 12. - Thrust coefficient for model F ram-jet engine with indicated values of $\mu^2 \tau$.

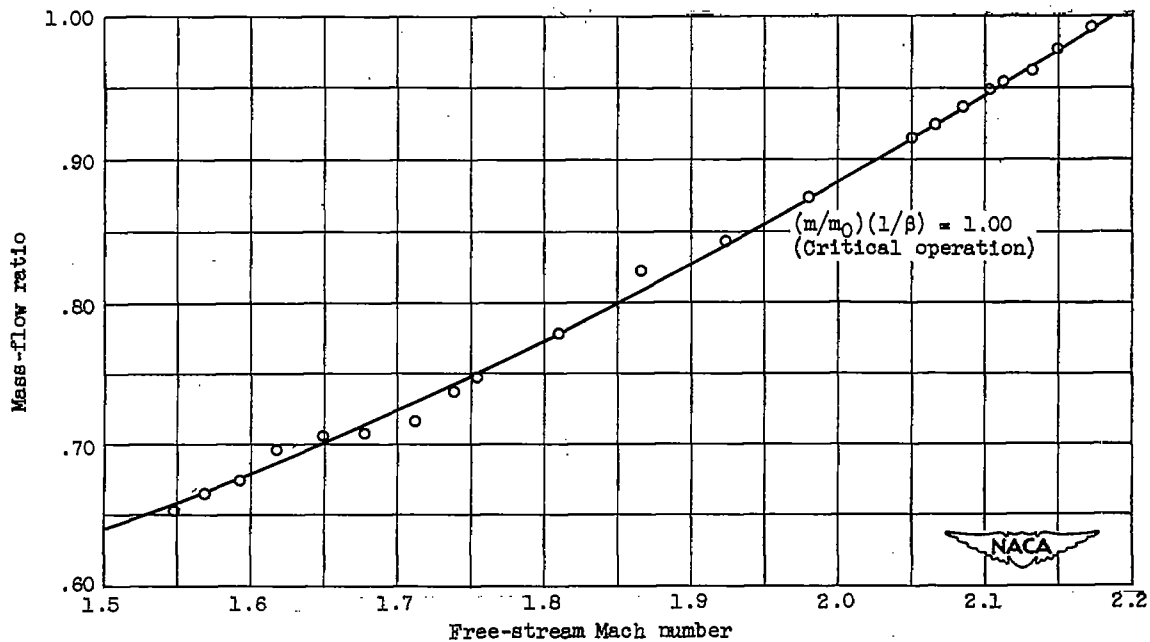


Figure 13. - Mass-flow ratio for model F ram-jet engine with critical operation line superimposed on data points.

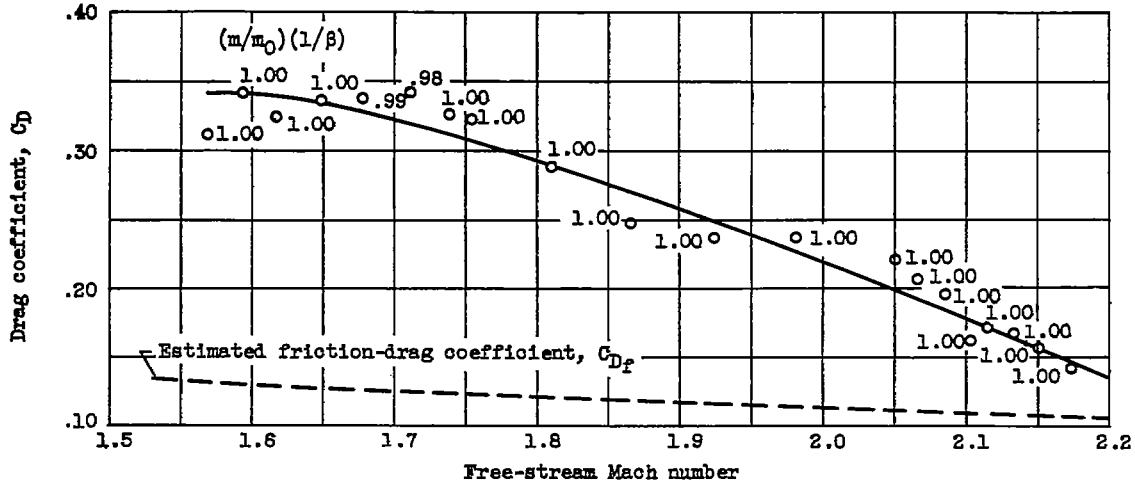


Figure 14. - Total-external-drag coefficient for model F ram-jet engine with indicated values of $(m/m_0)(1/\beta)$.

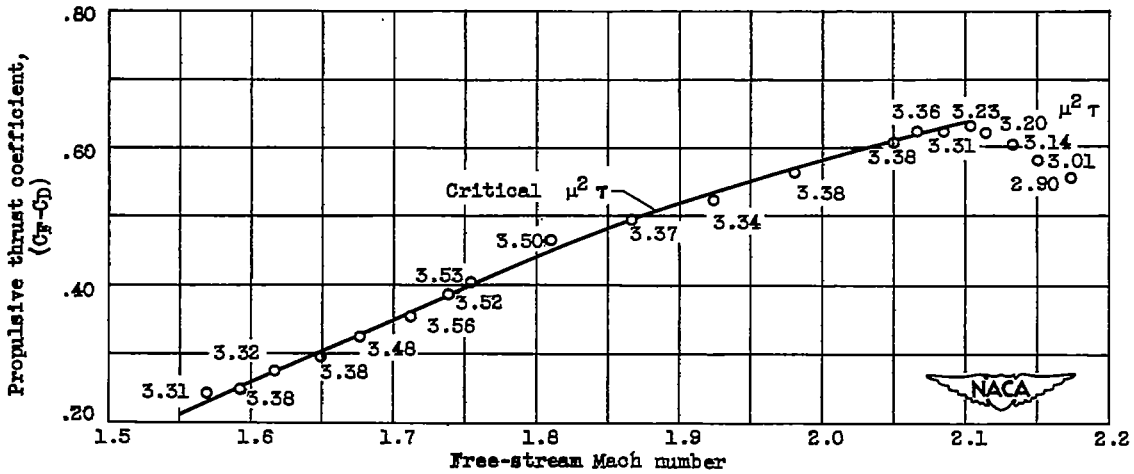
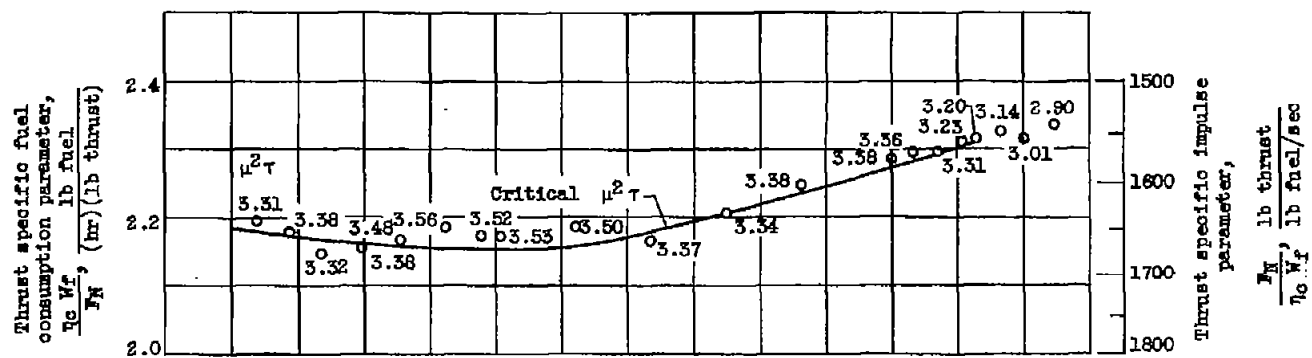
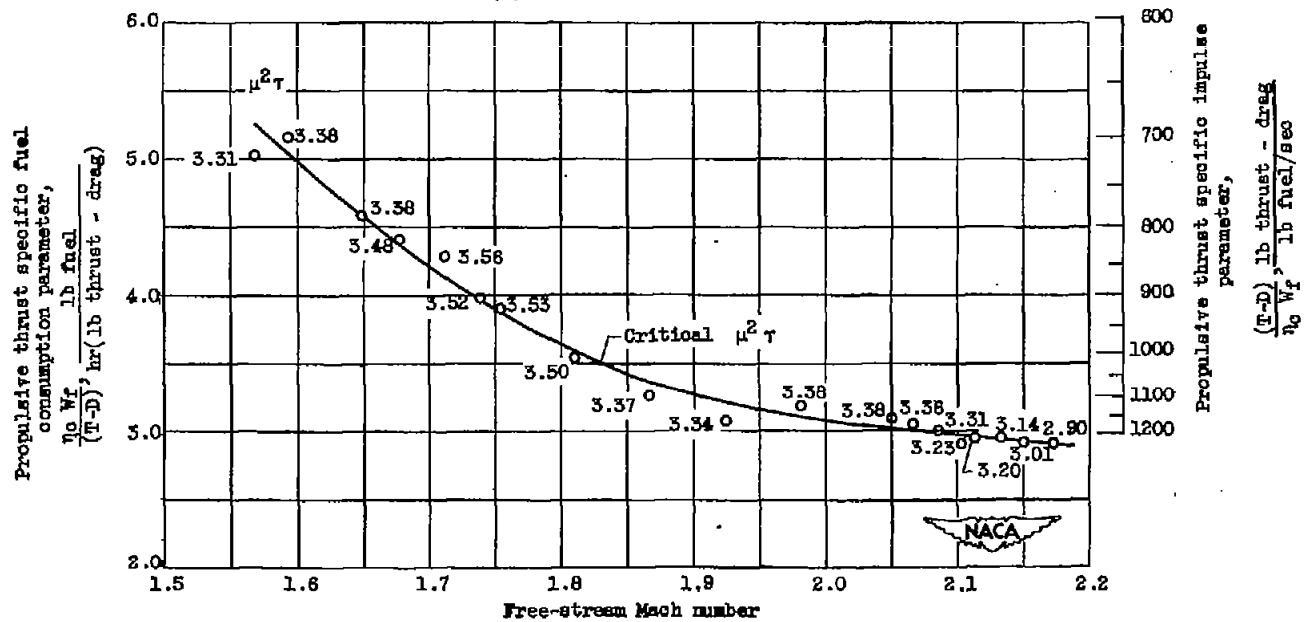


Figure 15. - Propulsive-thrust coefficient for model F ram-jet engine with indicated values of $\mu^2 T$.



(a) Based on net thrust.



(b) Based on propulsive thrust.

Figure 18. - Specific fuel consumption and specific impulse for model F ram-jet engines with indicated values of $\mu^2 \tau$.

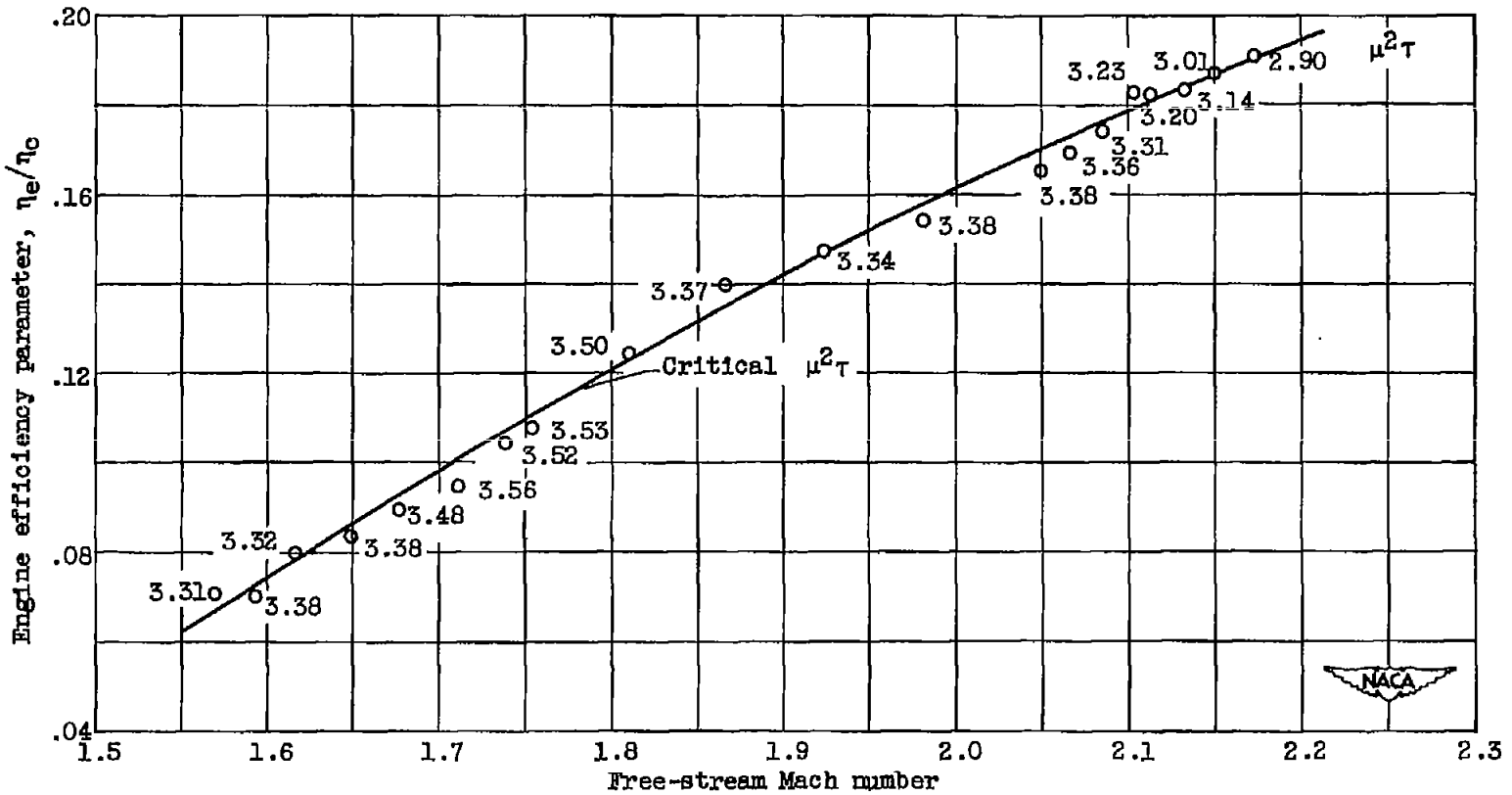
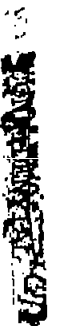


Figure 17. - Over-all ram-jet engine efficiency corrected to 100 percent combustion efficiency for model F ram-jet engine with indicated values of $\mu^2\tau$.